International Journal of Heat and Technology
Vol. 42, No. 5, October, 2024, pp. 1567-1577
Journal homepage: http://iieta.org/journals/ijht

Numerical Study of Heat Transfer in Helical Cone Coil Heat Exchanger Using MWCNT-Water Nanofluid

Ali A. Nadhim[1*], Nabeh Alderoubi[2], Ola Hussein Ali Al-Tamermi[3], Mustafa Abdul Salam Mustafa[4], Hasan Shakir Majdi[5]

[1] College of Technical Engineering, A1-Farahidi University, Baghdad 10001, Iraq
[2] Design and Drafting Technology Department, Lincoln Campus, Southeast Community College, Lincoln 68521, USA
[3] Department of Mechanical Engineering, University of Wasit, Al-Kut 52001, Iraq
[4] Department of Refrigeration and Air Conditioning Engineering, Al-Rafidain University College, Baghdad 10001, Iraq
[5] Department of Chemical Engineering and Petroleum Industries, Al-Mustaqbal University College, Hillah 51001, Iraq

Corresponding Author Email: ali.asaad@uoalfarahidi.edu.iq

https://doi.org/10.18280/ijht.420510

Received: 13 May 2024
Revised: 12 August 2024
Accepted: 30 August 2024
Available online: 31 October 2024

Keywords:
multiphase, nanoparticles, fraction factors, Nusselt number, flow velocity

ABSTRACT

By using two-phase Eulerian model, authors numerically examined helical cone coil heat exchanger MWNCT/water nanofluid flow and thermal properties. Nusselt number, Reynolds number, heat transfer coefficient, pressure drop in different concentrations, volume fractions, and different flow rates done by using ANSYS fluent software. k-epsilon turbulence model employed in this simulation. By considering heat transfer and pressure drop properties, nanofluid performance factor was assessed. This study utilizes ANSYS multiphase technology to numerically evaluate multi-wall carbon nanotube (MWCNT)/water nanofluids heat transfer and pressure drop as they pass through helically cone coil tube heat exchanger. The authors utilized MWCNT/water nanofluid with 0.1%, 0.3%, and 0.5% particle volume fractions for fluid simulation. The simulations conducted using turbulent flow within 2200 to 4200 Dean number range. Study discovered that highest overall heat transfer coefficient 56% more that of water while using 0.5% nanofluid concentration and 4200 Dean number. Heat transfer coefficient improvement in 0.1%, 0.3%, and 0.5% MWCNT/water nanofluid concentrations correspondingly 17%, 34%, and 47% higher compared to water. The Nusselt numbers show a significant increase of 26%, 49%, and 65% when compared to water, at 0.1%, 0.3%, and 0.5% MWCNT/water nanofluids concentrations, respectively. The pressure decreases of nanofluids with concentrations of 0.1%, 0.3%, and 0.5% were 18%, 33%, and 45% greater than that of water, respectively.

1. INTRODUCTION

Helicoidal coil heat exchanger extensively employed in various industrial applications, chemical and food processing, power generation, electronics, environmental engineering, manufacturing, HVAC, waste heat recovery, cryogenic processes, and space applications among represented industries. Compact design, optimal mass and heat transfer coefficients, and small residence time distributions make helical coils widely employed in heat exchangers and reactors. Helical tubes' flow changed by centrifugal forces (Dean roll cells, [1, 2]). Secondary flow field, formed by curvature of tube, is characterized by circulatory motion that draws fluid particles toward the tube's center. Secondary flow improves heat transfer rate by reducing temperature gradient across tube's cross-section. There is a secondary convective heat transfer mechanism in this design that operates in the inverse direction of the main flow, setting it apart from conventional heat exchangers. Fluid flow and heat transmission examination in helical pipe has been provided by prior studies [3-5]. When contrasted with mountain of heat transfer in coiled tubes literature, research papers amount on outside heat transfer coefficient shockingly low. Figueiredo and Raimundo [6], Haraburda [7], Prasad et al. [8], and Patil et al. [9] discussed design techniques for coil inside shell heat exchangers that use helically coil tubes as banks of straight tube to calculate outside heat transfer coefficient.

Research into methods of heating a coiled tube is, thus, ongoing. Various types of tubes, coil diameters, pitches, and turns are only a few of the design parameters that have been the subject of research into their impact on heat transmission and pressure reductions [10-12]. Dead zones, in which heat transfer does not take place because fluid is not flowing, are more likely to occur in shell-and-coil heat exchangers due to their complex construction. Because of the dead zone's effect on heat transport, thermal efficiency is decreased. However, these zones are superfluous in helical pipe coil heat exchangers since working fluid is always perfectly in touch with surface area of exchanger. Furthermore, generating a secondary flow propelled by curved annular tube, the heat transfer

performance can enhance even further. nanofluid presented by Choi and Eastman exhibits dissipation stability and excellent thermal characteristics, namely with high thermal conductivity [13]. Many researchers investigated various nanofluids thermal characteristics [14-16]. Various kinds of heat exchangers and operating conditions have been analyzed with these qualities to learn crucial flow and heat transfer characteristics. To accurately evaluate increased heat transfer using nanofluids, however, the proper tests are required, such as creating uniformly distributed nanofluids and establishing a visualization for the flow phenomena. Due to the intricacy of the experimental technique, numerical studies on nanofluid heat transport are necessary. Past research has shown that numerical methods used for single-phase scenarios are capable of producing reliable predictions of heat transfer characteristics [17, 18]. To understand the behavior of particles in nanofluids, two-stage research may be necessary before their practical use (e.g., particle dispersion) inside flow field. Microchannels [19], single helical coils [20], annuluses, conventional tubes, and their simplified domains have been the dominant shapes in two-phase numerical examinations of nanofluid heat transfer properties up until this point. In more complex numerical experiments, such as those involving heat exchangers with two pipes and helical coils, laminar flow ranges or the assumption of a single phase has been employed [21].

Kalb and Seader [22] performed numerical investigations about helical coil heat transportation using orthogonal toroidal coordinate system in uniform heat flow case. For Prandtl numbers >0.7, they found that local Nusselt number in inner wall area always less than straight tube and went downhill as Dean number increased up to certain limit. Zapryanov et al. [23] used a fractional step method to quantitatively investigate developed laminar flow and heat transfer over wide range of Prandtl (0.005 to 2000) and Dean (10 to 7000) values. Focusing on the case when the wall temperature stays constant, they proved that Nusselt number increases with Prandtl number, even while Dean number fixed. Spiral coils were underappreciated compared to helical ones, even though the former performed better in reported results [24]. Naphon and Suwagrai [25] investigated curvature ratios impact in horizontally spirally coiled tubes heat transport using numerical and experimental approaches. In comparison to straight tube, Nusselt number and pressure drop in spirally coiled tube 1.49 and 1.50 larger, respectively, due to centrifugal force. Research numerically investigated heat transfer, velocity, Dean, Nusselt number characteristics of cone helical coil heat exchanger for multi-wall nano carbon tubes (MWNCT)/water.

Nanofluid material known for its high thermal conductivity and stability over various points during time using two-phase Eulerian model to circumvent these limitations. Furthermore, performance factor calculated based on heat transfer and pressure drop characteristics to assess energy efficiency.

Study explores effectiveness in improving helical coil heat exchangers' heat transfer with using MWCNTs nanofluid and adopts complicated Eulerian model to simulate nanofluid flow and heat properties, this technique greater accurate than single models, because it captures the dynamics of nanoparticle dispersion and heat switch in the fluid. The studies introduce calculation of performance factor that mixes results of heat transfer enhancement and pressure drop. This element is crucial for comparing the overall strength efficiency of the nanofluid within the heat exchanger and provides a clear metric for evaluating the performance of various nanofluid concentrations. The study not just handiest performs numerical simulations but also validates its findings in opposition to current experimental records. This validation enhances credibility of effects and confirms accuracy of numerical model, taking a look at dependable references for destiny studies within area.

2. NUMERICAL METHOD

2.1 Two phase model

In its two phase numerical model, Euler Lagrangian and Euler Euler methods both used. After applying Euler-Lagrangian method, fluid was thought of as continuous surface. Due to their status as an independent phase, the fluid particles' tracking was incorporated into the simulation. It is possible to transfer mass, energy, and motion via the continuum and the interactions of individual particles. A powerful computer is required to do the simulations of all nanoparticles in the computational area using the Euler-Lagrangian method [17]. All phases, whether they are particles or fluids, are simultaneously seen as pervasive continuums in Euler-Euler method, which extends across the whole computational domain. No other phase occupies volume fraction of initial phase. Heat transmission properties of nanofluids forecasted using Euler-Euler method and commercial tool called ANSYS Fluent 18.1.

The preference between Euler-Lagrangian and Euler-Euler methods relies upon the specific requirements of the simulation. The Euler-Lagrangian method is most suitable for exact simulations in which individual particle dynamics are critical, however, it requires greater computational strength. On the opposite hand, the Euler-Euler technique is more appropriate for big-scale simulations in which the focal point is on the overall conduct of the phases in place of character particles. These techniques are vital to modern CFD software programs like ANSYS Fluent, enabling engineers and researchers to expect and optimize the behavior of complex multi-segment structures in diverse commercial programs, such heat exchangers, chemical reactors, and fluidized beds. Understanding strengths and obstacles of every approach is key to choosing the right version for a given problem.

The two multi-phase models available inside ANSYS Fluent are volume of fluid (VOF), mixture, and Eulerian. VOF system functions in fixed grids by use of surface tracking method. It is common practice to use this model for stratified flows and free-surface movements. When relative velocities of the various phases are compared, mixture momentum equation is found using mixture model. Within this mixing model, both bubble fluxes and particle flows are taken into account. Each step in the Eulerian model is treated separately when solving for momentum, energy, and continuity. Phase transitions can occur between fluid-solid or solid-solid states, depending on the pressure and exchange coefficient. To represent helical cone coil heat exchangers nanofluids' heat transfer properties, authors relied on Eulerian model to determine particle phase and base fluid phase controlling equations [26]. Continuity equation, or mass conversion equation, is demonstrated by Eqs. (1) to (3):

$$\nabla.\left(\varphi_l\,\rho_l\,\underset{v_l}{\rightarrow}\right)=0 \tag{1}$$

$$\nabla.\left(\varphi_s \rho_s \underset{v_s}{\rightarrow}\right) = 0 \tag{2}$$

$$\varphi_1 + \varphi_2 = 1 \tag{3}$$

(l) and (s) stand for liquid and solid phases. liquid phase momentum equation for (l) is:

$$\nabla.\left(\varphi_l \rho_l \underset{v_l}{\rightarrow}\underset{v_l}{\rightarrow}\right) = -\varphi_l \nabla P + \nabla.\bar{\tau_l} + \varphi_l \rho_l \vec{g} + \sum_{s=1}^{n} \overrightarrow{R_{sl}} + \left(\overrightarrow{F_l} + \overrightarrow{F_{llft,l}} + \overrightarrow{F_{vm,l}}\right) \tag{4}$$

(P) represented shared pressure of all phases. $\overrightarrow{F_l}, \overrightarrow{F_{llft,l}}, and\ \overrightarrow{F_{vm,l}}$ external body force, lift force, and virtual mass force. Viscous stress tensor $\bar{\tau_l}$, expressed using Eq. (5).

$$\bar{\tau_l} = \varphi_l \tau_l \left(\nabla v_l + \nabla \vec{v_l^T}\right) + \varphi_l \left(\lambda_l - \frac{2}{3} u_l\right) \nabla.\vec{v}_l I^{=} \tag{5}$$

Interphase momentum force (i.e., volume force induced on each phase by other), $\vec{R}_{sl}$, determined using Eq. (6).

$$\sum_{s=1}^{n} \overrightarrow{R_{sl}} = \sum_{s=1}^{n} K_{sl}(\overrightarrow{v_s} - \overrightarrow{v_l}) \tag{6}$$

where, *Ksl* represents interface transfer coefficient momentum. Solid phase momentum equation for (s) is:

$$\nabla.(\varphi_s \rho_s \overrightarrow{v_s}\ \overrightarrow{v_s}) = -\varphi_s \nabla P + \nabla P_s + \nabla \bar{\tau_s} + \varphi_s \rho_s \vec{g} + \sum_{l=1}^{n} K_{ls}(\overrightarrow{v_l} - \overrightarrow{v_s}) + \left(\overrightarrow{F_s} + \overrightarrow{F_{llft,s}} + \overrightarrow{F_{vm,s}}\right) \tag{7}$$

P_s defines solid pressure generated by particle collusion. Interface momentum transfer term in momentum equation refers to drag force. Interface momentum transfer coefficients (K_{sl} and K_{ls}) determined using Wen and Yu model [27]:

$$K_{sl} = K_{ls} = \frac{3}{4} C_D \frac{\varphi_s\ \varphi_l\ \ \rho_l\ |\overrightarrow{v_l} - \overrightarrow{v_s}|}{d_s} \varphi_l^{-2.65} \tag{8}$$

$$C_D = \frac{24}{\varphi_l\ Re_s}[1 + 0.15(\varphi_l\ Re_s)^{0.678}] \tag{9}$$

$$Re_s = \frac{\rho_l\ d_s\ |\overrightarrow{v_s} - \overrightarrow{v_l}|}{\mu_l} \tag{10}$$

2.2 Conditions for boundaries and simulation geometry

This investigation used a three-dimensional flow domain to estimate nanofluid Nusselt number, heat transfer coefficient, and pressure drops using Eulerian two-phase model. This allowed us to study heat transfer features of MWNCT nanofluid in helical cone coil heat exchangers. MWNCT nanofluid simulated by calculating its steady-state heat transfer and hydraulic properties. Figures 1, and 2 show shell and cone helical coil heat exchangers in three dimensions, respectively. Helical cone coil was supplied with cold fluid (i.e., 10°C) and shell with hot fluid (i.e., 60°C). Cold side carried nanofluids while hot side carried water. There was flow counter between two fluids. Specific dimensions of heat exchanger can be found in Table 1. It was thought that adiabatic boundary of shell would be located on its exterior, or hot side. Table 2 displays MWNCT/water components characteristics utilized in this research, including nanoparticles and water itself. Third-order polynomial equation utilized to represent precise thermal characteristics throughout heat transfer, as water's properties vary with temperature [28]. Tables 2 and 3 show simulation conditions and numerical methods of this study. helical cone coil walls and shell applied like no slip boundary conditions. Uniform flow applied for inlet, temperature and mass flow rate also employed. Mass flow rate on cold side set to 0.07kg/sec.

While hot side mass flow rate was fixed at 0.17kg/sec. Hot and cold outlets applied to zero-pressure conditions. The wall of the helical cone coil and the shell were modeled with non-slip boundary situations. This implies that fluid velocity on wall is 0, relative to wall surface. Outside of shell became assumed to be adiabatic, which means no heat transfer happens through the outer shell surface. The simulation assumed constant wall heat flux at tube's border, making sure of steady thermal conditions throughout the heat transfer process. Turbulent intensity (I) was estimated for each scenario. This is used to calculate the initial turbulent portions (k and ε) for the simulation. These boundary situations have been carefully selected to mimic realistic running situations inside a helical cone coil heat exchanger, ensuring that the simulation outcomes can be efficaciously validated against experimental records.

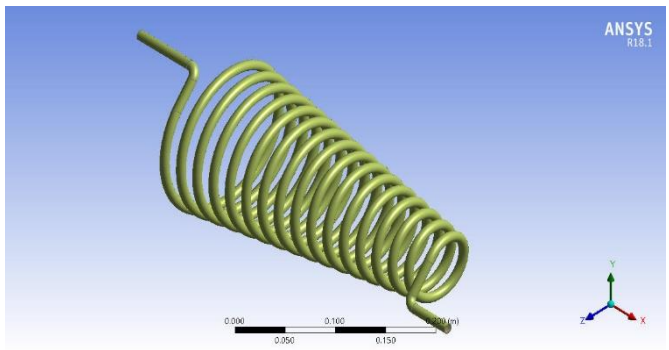

Figure 1. Geometry design of cone helical coil heat exchanger

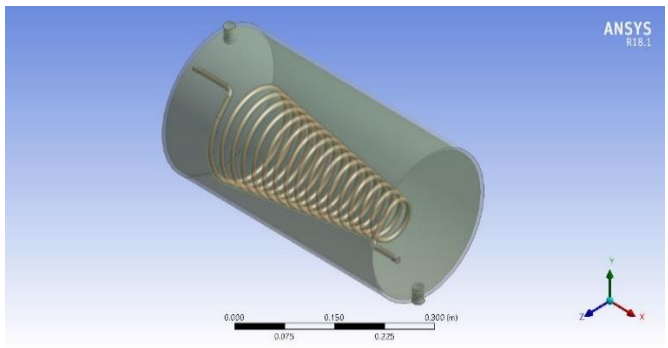

Figure 2. Cone helical coil heat and shell exchanger geometry design

Table 1. Cone coil tube and shell dimensions

Coil Angle (Θ)	8 Degrees
Inner tube diameter (Di)	0.8 cm
Outer tube diameter (Do)	1 cm
Shell diameter	11.4 cm
Effective length	470 cm
Coil pitch	2 cm
Calming section length	11 cm
Coil diameter	6.4 cm
Turns number	16

Table 2. MWCNTs Nanopowder thermophysical properties

Solution Method	Model or Scheme
Turbulence model	Realizable k-epsilon
Near wall treatment	Enhanced wall treatment
Pressure-velocity	coupling PC-SIMPLE
Gradient	Least-Squares Cell-Based
Momentum	QUICK
Volume fraction	QUICK
Turbulent kinetic energy	Power law
Turbulent dissipation rate	Power law

Table 3. Numerical method employed in the present study

Form	Solid
Outer (Di.)	50-80 nm
Inner (Di.)	5-15 nm
length	10-20 μm
Specific surface area	32-40 m^2/g
True density	2.1 g/cm^3
Bulk density	1.8 g/cm^3
Purity	99.5%
Thermal conductivity	3000 W/mK

2.3 Mesh selected test

A high-quality discretization is directly proportional to the finite volume method's accuracy. Structured hexahedral meshes, which are known to offer better accuracy while reducing CFD computational effort, were employed in this investigation. To verify that mesh resolution affected outcomes and to reduce numerical impacts caused by mesh size and distribution, thorough mesh sensitivity analysis was conducted. In Figure 3, the authors can see the heat exchanger's mesh in its calculation domain. Through execution of mesh independence tests, this particular mesh scenario was chosen. Because it impacts Y+values, which in turn impact the Nusselt number computation throughout the simulation, mesh cell size is critically significant in multi-phase fluid modeling. The dimensionless wall distance parameter used in computational fluid dynamics (CFD) simulations is consulted by Y+values in ANSYS mesh validation. Its purpose is to determine the optimal mesh period close to a fluid's walls in conjunction with the drift location, to guarantee accurate simulation results. By looking at the Y+values, we can evaluate the boundary layer decision and check if the mesh is large enough to capture the wave physics close to the walls. In most cases, the sweet spot for maximal CFD simulations is a Y+charge of about 1. The following formula may be used to determine Y+values in ANSYS mesh validation:

$$Y+= \frac{(y \times \rho \times u)}{\mu} \tag{11}$$

where, Y+is dimensionless wall distance parameter, y is space from wall to the first cellular centroid, ρ is fluid density, u is speed of fluid, and μ is dynamic viscosity of fluid. By inputting the values for y, ρ, u, and μ into these components, users can calculate the Y values to evaluate boundary layer decision and ensure mesh is first-rate enough to seize the waft physics near the walls in ANSYS CFD simulations. The model simulation mesh has 4787563 elements and 1000738 nodes with 20 mm elements size.

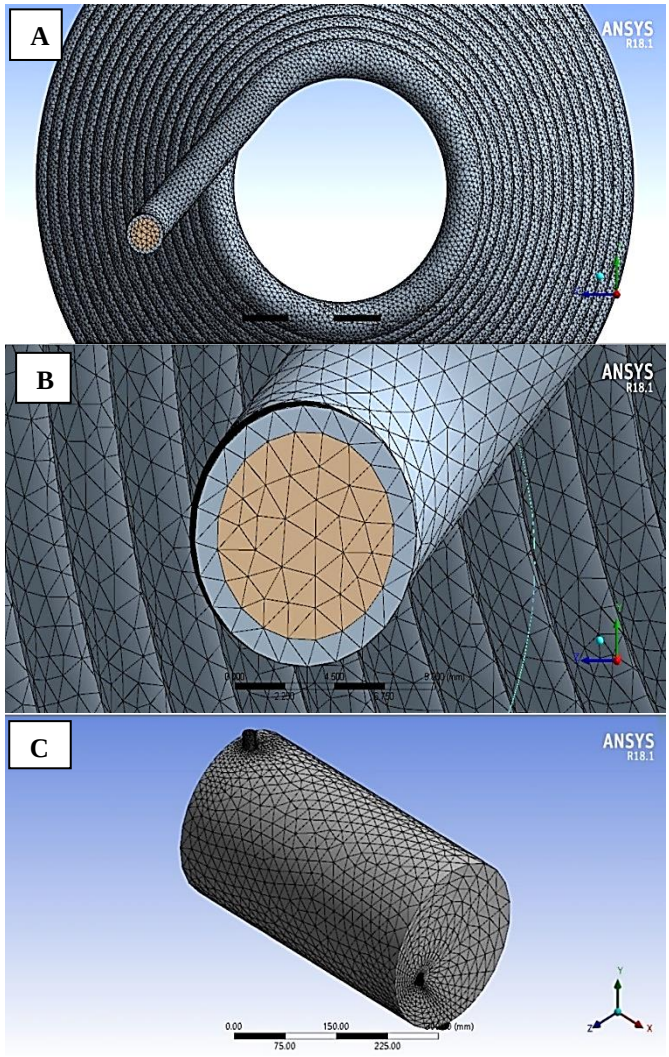

Figure 3. Simulation geometric mesh: (A) helical cone coil mesh, (B) MWNCT and tube mesh, (C) shell and coil mesh

2.4 Nanofluid thermal properties

Nanofluids thermophysical properties, namely viscosity μ_{nf}, density ρ_{nf}, thermal conductivity k_{nf}, and heat capacitance, $(\rho C_p)_{nf}$ proposed by Brinkman [29]. Eventually, Brinkman model presented in volume fraction in following equation:

$$\rho_{nf} = (1 - \emptyset)_{\rho f} + \emptyset_{\rho s} \tag{12}$$

where, ρf is density of fluid phase, ρs is density of solid phase, ∅ is volume fraction of solid phase in mixture, and (1-∅) is volume fraction of fluid phase in mixture:

$$(\rho C_p)_{nf} = (1 - \emptyset)(\rho C_p)_f + \emptyset(\rho C_p)_s \tag{13}$$

where, $(\rho Cp)_{nf}$ is specific heat capacity of fluid phase, $(\rho Cp)_s$ is specific heat capacity of solid phase, ∅ is volume fraction of solid phase in mixture, and (1-∅) is volume fraction of fluid phase in mixture:

$$\frac{k_{nf}}{k_f} = \frac{(k_s + 2k_f) - 2\emptyset(k_s + k_f)}{(k_s + 2k_f) + \emptyset(k_s - k_f)} \quad (14)$$

where, (k_{nf}) is effective thermal conductivity of two phase fluid mixture, *kf* is thermal conductivity of fluid phase, *ks* is thermal conductivity of solid phase, and ∅ is volume fraction of solid phase in mixture:

$$\mu_{nf} = \frac{\mu_f}{(1 - \emptyset)^{2.5}} \quad (15)$$

where, μf is fluid phase viscosity, and ∅ is solid phase in mixture volume fraction.

Nanofluid viscosity, density, thermal conductivity, and heat capacitance can be estimated using equations derived from nanofluid model; all that is required is base fluid viscosity substitution at given temperature. Table 4 displays pure water thermophysical characteristics at 293K. MWNCT/water fluid thermophysical properties presented in Table 5 for experimental three concentrations (0.1%, 0.3%, and 0.5%).

Table 4. Pure water thermophysical properties

Thermophysical Properties	Water
Density, (ρ) m^3/kg	998.21
Specific heat, (Cp) J/kg.K	4182
Thermal conductivity, W/m.K	0.6024
Dynamic viscosity, (μ) pa.s	0.001003

Table 5. MWNCT/water thermodynamics characteristics at various volume fractions

Thermophysical Properties	MWNCT Volume Fraction		
	0.1%	0.3%	0.5%
Density (ρ) m^3/kg	999.31	1001.53	1003.52
Specific heat (C_p) J/kg.K	4182.11	4180.19	4178.97
Thermal conductivity (k) w/m.K	0.6005	0.6076	0.6190
Dynamic viscosity (μ) pa.s	0.001005	0.001010	0.001015

2.5 Simulation boundary conditions

As input fluids for helical cone coil, MWNCT/water utilized volume fraction nanofluids at concentrations of 0.1%, 0.3%, and 0.5%. Operating fluid for shell was water. At both horizontal coil tube and shell entrance, a uniform velocity profile was used in simulation analysis. Turbulent quantities (k and ε), turbulent intensity (I) first estimate was given. Using formula I=0.16Re1/8 to calculate turbulent intensity for each scenario. At outlet border, outflow boundary conditions have been applied. Assuming constant wall heat flow at tube's border, simulation model wall is modeled as a smooth surface.

Mass flow rate of 0.15kg/sec. was measured at hot inlet and 0.07kg/sec. at cold inlet, with fluid entering at consistent 10°C for cold nanofluids of the cone coil and 60°C for shell hot water fluid. The intake pipe was used to profile flow rate. Thermal boundary conditions and Reynolds (Re) were selected so that they matched (Re) of existing correlations [30]. Relative average pressure of zero was determined at computational model's exit. Everyone thought walls were perfectly smooth from hydraulic standpoint. To determine (Re) values, authors will use nanoparticles/water fluid thermophysical characteristics at volume fractions ranging from 0.1% to 0.5%, following methodology similar to the study [31]. Turbulent flow with Dean number (De) between 2200 and 4200 was used for this simulation. The following equation describes (De) that ANSYS program uses to estimate Reynolds Number (Re):

$$D_e = \frac{R_e\, D}{2R} \quad (16)$$

where, R_e is Reynolds number, D is pipe diameter, and R is pipe curvature radius. Sequence of steps involved in ANSYS-FLUENT analyzed to determine Reynolds number depending on mean velocity (u) of working fluid from following Eq. (17). For present study, Reynolds number estimated according to 0.7kg/s inlet mass flow of MWNCT/water fluid. Mass flow converting to inlet velocity by using the following equation:

$$Mass\ flow\ rate = density \times velocity \times area \quad (17)$$

3. RESULTS AND DISCUSSION

3.1 Velocity effects profile

Due to centrifugal force generated by coil curvature, flow in helical cone coil heat exchanger significantly disturbed along its length. Irregular flow and difficulties in forecast were caused by this flow disturbance, which became dominant before completely formed region. As result, authors needed to locate completely established area to study helical cone coil heat exchanger's thermal properties.

Figure 4 displays velocity flow profiles contours along heat exchanger's coil length in three separate locations. Three cases were tested with cone coil fluid containing nanoparticles at concentrations of 0.1%, 0.3%, and 0.5% volume surfactant added using two-step method. Experiments carried out with turbulent flow within 2200<De<4200 Dean number range. According to following equation, Reynolds number computed by ANSYS FLUENT is modified by flow velocity inside pipe:

$$R_{e=}\frac{\rho u D}{\mu} \quad (18)$$

where, R_e is Reynolds number, ρ is nanofluid density, u is velocity, D is hydraulic diameter, and μ is nanofluid viscosity. All variables in the previous equation are constant for the same concentration except flow velocity which will control Reynolds number values.

The velocity ANSYS calculation results of the three concentrations along the coil cross-sections illustrated very small differences in nanofluid velocity between the three concentrations (0.1%, 0.3%, and 0.5%), the differences in velocity values between the three tested locations in Figure 5 explained due to the alteration in coil curvature which will affect the nanofluid velocity. The increase in velocity at the center and outlet sections due to decrease in helical coil curvature and increasing in nanofluid temperature due to heat exchanger between cold nanofluid inside coil and hot water outside it. The helical coil induces a secondary float because of centrifugal forces, which can be more potent close to the

coil walls. As the curvature decreases (i.e., the coil turns into much less curved), the centrifugal forces reduce, main to a greater uniform velocity distribution throughout the coil's cross-phase. In the center of the coil, wherein the curvature consequences are much less said, the fluid speed tends to be higher. This is due to the fact the fluid reports much less resistance in comparison to boundary layers near partitions of coil.

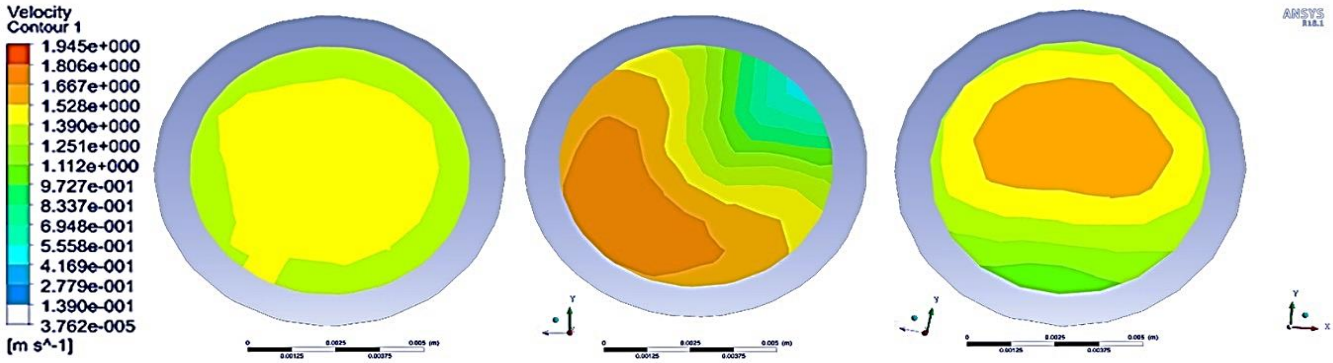

Figure 4. Axial profile velocity crossing cone coil pipe section in three locations using 0.3% MWNCT nanoparticle concentration (A) inlet (B) center (C) outlet

At hole section, the fluid velocity increases due to conservation of mass and momentum. As fluid exits coil, reduced curvature permits extra streamlined waft, minimizing electricity losses and keeping better velocities.

3.2 Relation between Dean number and Nusselt number

To forecast particle or base fluid velocities and temperatures, Eulerian two-phase model computes each phase governing equations (i.e., MWNCT and water phases). To examine nanofluids' two-phase heat transfer coefficient, it necessary to determine Nusselt numbers at side of coin coil where fluid flows. This may be done using the following equation in ANSYS software:

$$N_u = 0.023 Re^{0.8}\, Pr^{0.4} \tag{19}$$

where, *Nu* Nusselt number, *Re* Reynolds number, and *Pr* Prandtl number which defined dimensionless number that characterizes momentum diffusivity to thermal diffusivity in fluid ratio. According to previous Eq. (19), Reynolds number will control Nusselt number values which used for establish heat transfer coefficient (h) according to following equation:

$$N_u = \frac{hD_h}{K} \tag{20}$$

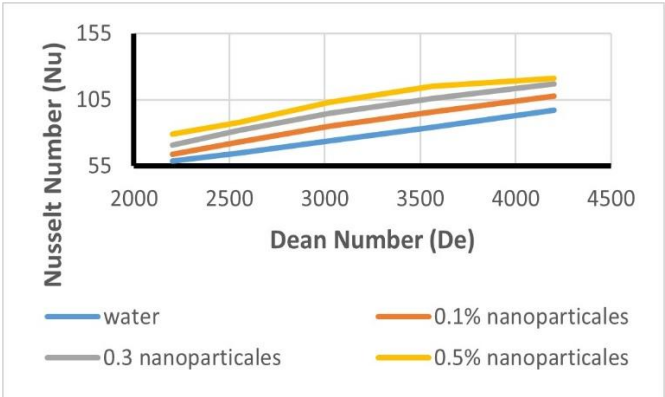

Figure 5. Nanoparticle concentration effect on nanofluids Nusselt number

where, *Nu* Nusselt Number, D_h is hydraulic diameter, a characteristic length scale used in fluid flow calculations, and h heat transfer coefficient. Calculated Nusselt number shows that experiment's nanofluid volume concentration of 0.1%, 0.3%, and 0.5% of produced Nusselt numbers 26%, 49%, and 65% higher than water Nusselt numbers as illustrated in Figure 5.

For each of three nanofluid concentrations, Figure 6 shows relationship between Dean (De) and Nusselt (Nu) numbers; figure also indicates that, according to Eqs. (16) and (18), there is direct proportion between these two values. Nanofluid density, which is proportional to concentration of nanoparticles in experimental fluid, is sole variable that differs among the three models. Dean number and particle volume concentration increase Nusselt number, as seen in Figure 5. Nusselt numbers grow by 26%, 49%, and 65% compared to water Nusselt numbers in nanofluids containing 0.1%, 0.3%, and 0.5% MWCNTs, correspondingly.

Mixing of water particles with CNTs, which may be a result of Brownian motion of CNTs, is responsible for improvement. Additionally, MWCNTs' haphazard mobility enhances development of secondary flows and disrupts creation of boundary layers. Because it directly proportional to inner heat transfer coefficient, Nusselt number grows as heat transfer coefficient and volume concentration both rises. An important Nusselt value represents efficiency of convective heat transfer. When particle volume concentration increases, convective heat transfer proves to be incredibly effective method in this study.

3.3 MWCNT nanofluids heat transfer properties

Figure 6 shows relationship between Dean number and heat transfer coefficient. When particles volume concentration and Dean number increase, total heat transfer coefficient also increases. With 0.5% nanofluid concentration and 4200 Dean number, highest total heat transfer coefficient was 56%. Combined impact of heat exchanger's conduction with convection modes is total heat transfer coefficient. When comparing the two modes of heat transfer, convection far more efficient than conduction. The enhanced convection current between the water and MWCNTs makes the internal heat transfer more efficient. As a result, convective heat transport

is enhanced. Convective heat transmission is greatly enhanced since the temperature differential between the shell and tube is reduced.

Impact of particle concentration on coefficient of heat transmission leads to heat transfer coefficient rising trend when Dean number changes. At 0.1%, 0.3%, and 0.5% MWCNT/water concentrations, heat transfer coefficient enhancement was 17%, 34%, and 47% higher than water, correspondingly. When nanofluid concentration 0.5%, the heat transfer coefficient reaches its maximum. Thermal conductivity of nanofluids enhanced when MWCNT amount increased. Furthermore, the inclusion of MWCNT causes the temperature profile to flatten and postpones the creation of the thermal boundary layer. At 0.5% volume concentration, increasing in inner heat transfer coefficient resulted from both thermal boundary layer delaying effect and MWCNTs particles in water velocity reducing along curved flow route.

Figures 7(A) and (B) offer velocity and temperature profiles of water and nanofluids in helical heat exchanger. Both (A) and (B) of Figure 8 displays velocity and temperature distributions for nanofluid coil. Figures show how nanoparticles improve heat transfer and velocity relationship in helical heat exchanger. Nanofluids cause a noticeable rise in water temperature when compared to plain water. As an example, the water temperature rises by 3% when a 3% particle concentration level is present. The results show that temperature of nanoparticles/water fluid increases with increasing particle concentration and that it decreases with increasing water mass flow rate. This suggests that nanoparticles' ability to absorb heat makes water fluid hotter than it would be without them. ANSYS software can determine heat absorbed by nanoparticles/water fluid from measured temperatures using the two equations shown below:

$$Q_{nf} = m_{nf} C_{p,nf} \left(T_{nf,in} - T_{nf,out}\right) \tag{21}$$

$$Q_w = m_w C_{p,w} \left(T_{w,out} - T_{w,in}\right) \tag{22}$$

where, Q_{nf} represents heat transfer rate for nanofluid, m_{nf} represents mass flow rate of nanofluid, $C_{p,nf}$ represents specific heat capacity of nanofluid, $T_{nf,in}$ represents inlet temperature of nanofluid entering the system, and $T_{nf,out}$ represents outlet temperature of nanofluid leaving the system.

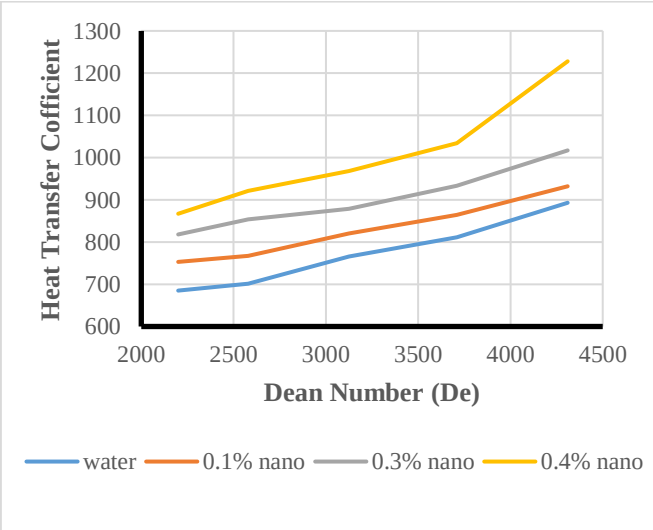

Figure 6. Heat transfer coefficient Vs Dean number

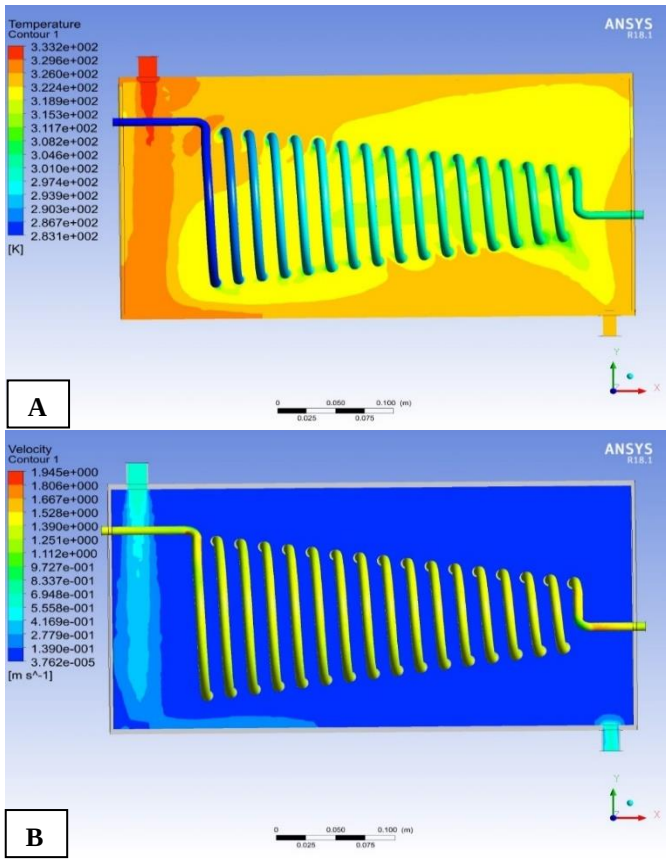

Figure 7. Nanofluids and water velocity and temperature profiles in helical and shell heat exchanger (A) temperature, (B) velocity

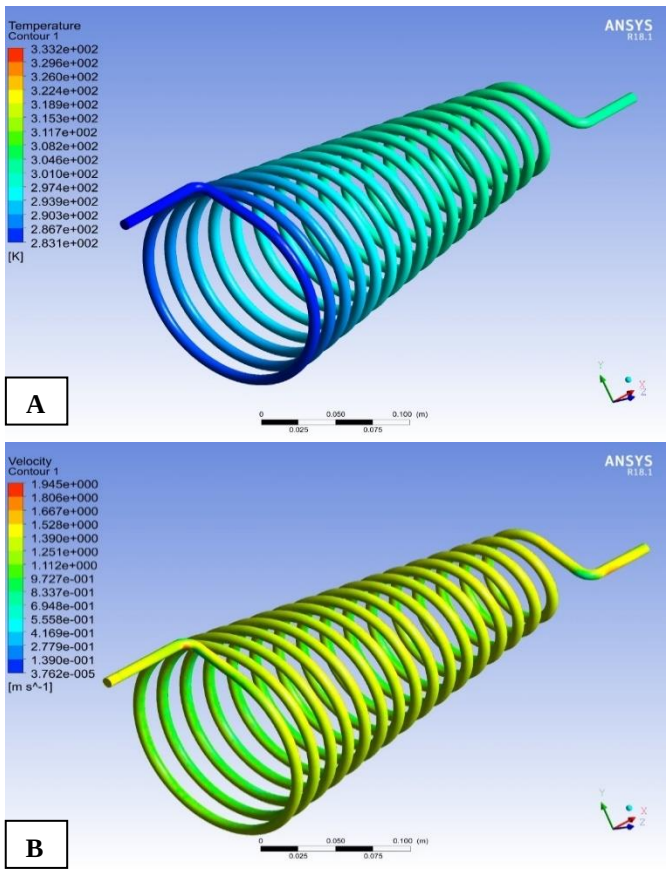

Figure 8. Velocity and temperature distributions for the nanofluid coil (A) temperature, (B) velocity

3.4 Pressure drops

Heat transfer and hydraulic properties represented by pressure drop determined pumping power and must be considered when using nanofluids in heat exchangers. To keep operations running normally, pump system would need to be redesigned to account for shifts in working fluids. As a result, authors looked at pressure drop for several scenarios, including different concentrations and flow rates. Pressure drops and friction factors are shown in Figures 9 and 10 for different concentrations and flow velocities. The simulation results show that pressure loss increases as particle volume concentration and Dean number fluctuate. Results show that nanofluids with concentrations of 0.1%, 0.3%, and 0.5% have pressure drops is 18%, 33%, and 45% more than water. The pressure loss grew as Dean's number or flow rate rose.

When flow rate increases, pressure drop also increases correspondingly, as seen by relationship between two variables ($\Delta P \propto u^2$). Pressure drops proportional to an increase in flow rate. This is caused by high fluid velocity, which leads to greater turbulence and a considerable dynamic pressure loss. Since density and viscosity of fluid both increase with increasing concentrations of nanofluid, pressure drop likewise climbed with increasing concentrations. Table 2 shows that the density of the MWNCT nanoparticle was high. Researchers have shown that nanofluid viscosity rises with concentration in previous research [32, 33]. The results suggested that the high density of the MWNCT nanofluid caused an increase in flow resistance, leading to a substantial pressure drop. Here is the formula for calculating the friction factor:

$$f = \frac{D_h \Delta P}{2L\rho u^2} \tag{23}$$

where, f represents friction factor, D_h is hydraulic diameter of pipe, ΔP pressure drop across pipe, (L) is pipe length, ρ is fluid density, and (u) is fluid velocity through pipe. Figure 10 shows that friction factor was less at 0.5 vol.% nanofluid compared to 0.3% and 0.1% vol. which means friction will be inversely proportional with (De) and by sequence with pressure drop. Pressure drop was higher because of high viscosity and density of fluid, even if friction factor was low at high concentration. Thus, higher nanofluids concentration would lead to higher pressure drops since flow resistance is improved because fluid density and viscosity are both increased (DP∝μ, ρ).

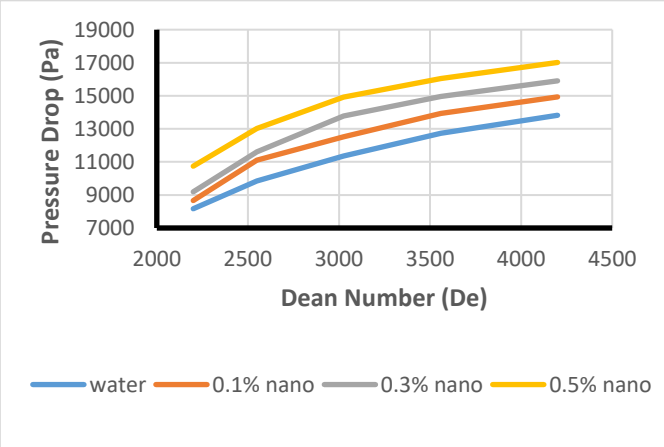

Figure 9. Nanofluid's effect on pressure drops

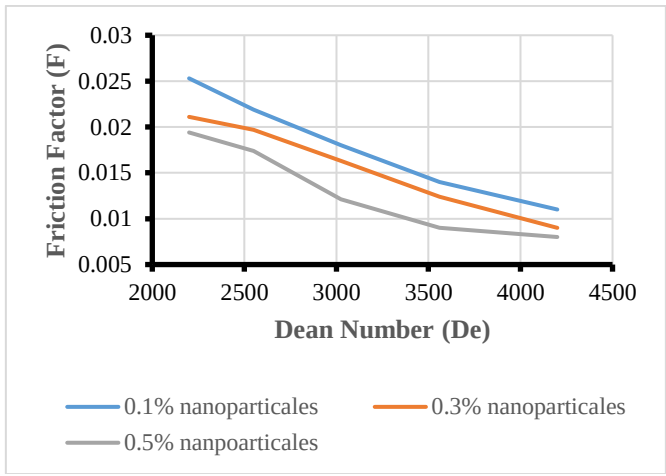

Figure 10. Pressure drops per friction factors on coil side for Dean number

3.5 Evaluating nanofluid energy efficiency

Evaluating energy efficiency of nanofluid can done by calculating performance factor (PF) using Nusselt number and pressure drop. Performance factor was calculated according to following equations:

$$PF = \frac{N_{uNF}/N_{uW}}{(f_{NF}/f_W)^{1/3}} \tag{24}$$

$$\frac{f_{NF}}{f_W} = \frac{\Delta P_{NF}/\rho_{NF}}{\Delta P_w/\rho_W} \tag{25}$$

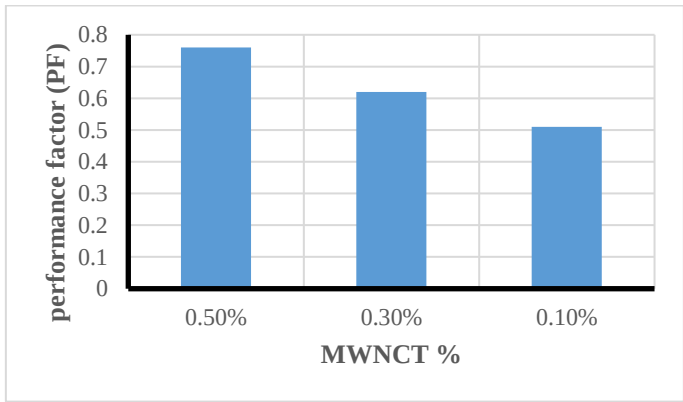

Figure 11. Performance factor of nanofluids at different concentrations

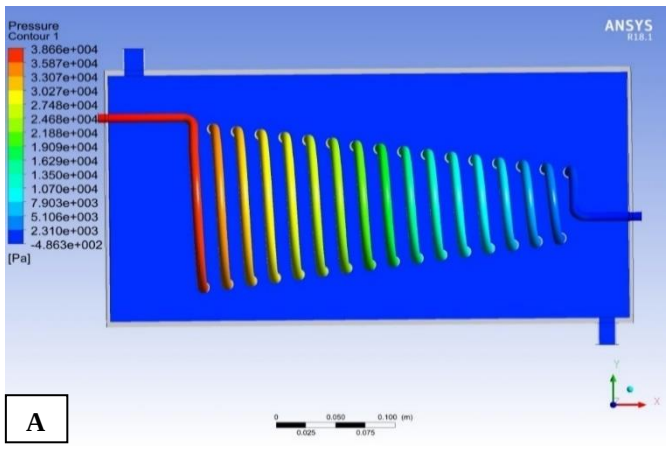

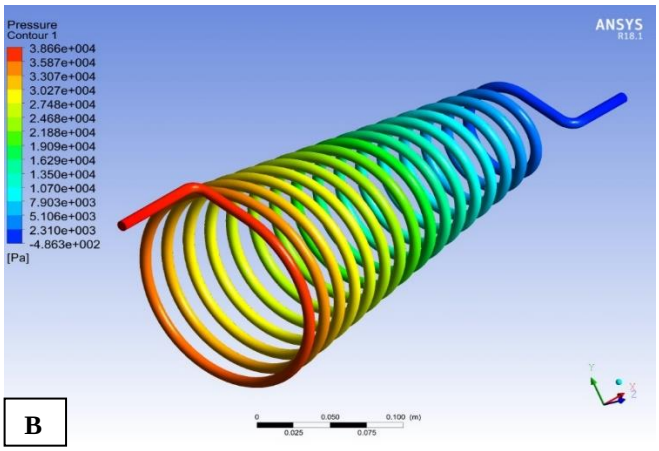

Figure 12. Pressure contour values (A) shell and coil (B) nanofluid coil

where, N_{uNF} is Nusselt number for the nanofluid, N_{uW} is Nusselt number for base fluid (without nanoparticles), f_{NF} is volume fraction of nanoparticles in nanofluid, f_W is nanoparticles volume fraction, ΔP_{NF} represents nanofluid pressure drop in system, ρ_{NF} represents density of nanofluid, ΔP_W represents pressure drop of base fluid (water), and ρ_W represents the density of base fluid (water). Figure 11 shows enhancement of performance when using the nanofluid inside the coil compared with the water. The Performance factor quantifies the extent to which heat transfer performance enhances about rise in pressure drop of nanofluid. Figures 12(A), and (B) depict a decrease in pressure within shell and coil containing nanofluid. Performance factor exhibited positive correlation with concentration, as both pressures drop and Nusselt number saw an increase. To clarify, enhancement in efficiency of heat transfer, which surpassed increase in pressure drop, greatly enhanced performance factor. This study focuses on evaluating performance factor of specific heat transfer system, namely helical coil heat exchanger. It is important to note that values obtained may vary for different heat transfer systems, depending on factors such as type of nanofluid, nanoparticle size, and concentration levels.

3.6 Validation

The validation of the mathematical model results was done by comparing it with the experimental results from previous research [34]. According to the ANSYS results the variation between the experimental and mathematical models for different nanofluid concentrations was between 1% to 3% due to the variation in flow rate and the outer conditions. Comparing the values of Dean and Nusselt's numbers between the present numerical study and the previous research is essential in predicting the results. Based on these findings, the two-phase Eulerian model used in this paper could be expected to accurately predict nanofluid heat transfer characteristics in different concentrations. Figures 13-15 illustrate the differences between the experimental work of reference [35] and the ANSYS analytical model results of the present work for heat transfer coefficient, pressure drop, and friction factor.

ANSYS simulation results 0.3 to 0.4% divergent from the experimental results for the heat transfer coefficient, pressure drop, and friction factor for (0.1, 0.3, and 0.5% nanoparticles concentrations). This small divergence reflected the accuracy of the simulation models in calculating the nanoparticle's percentage effects on the heat exchanger efficiency.

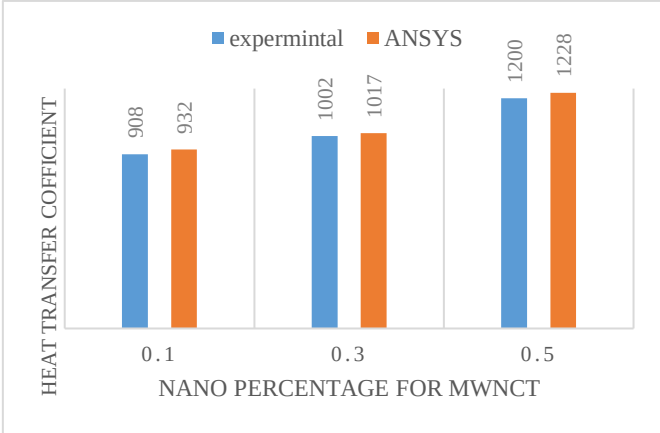

Figure 13. Heat transfer coefficient of the three nanoparticles concentration

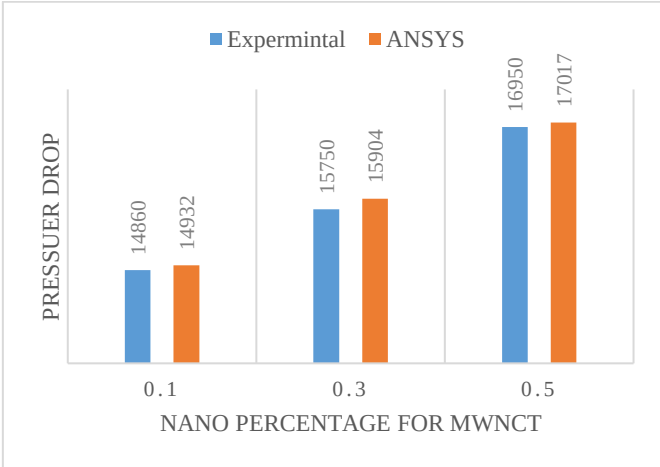

Figure 14. Pressure drop of the three nanoparticles concentration

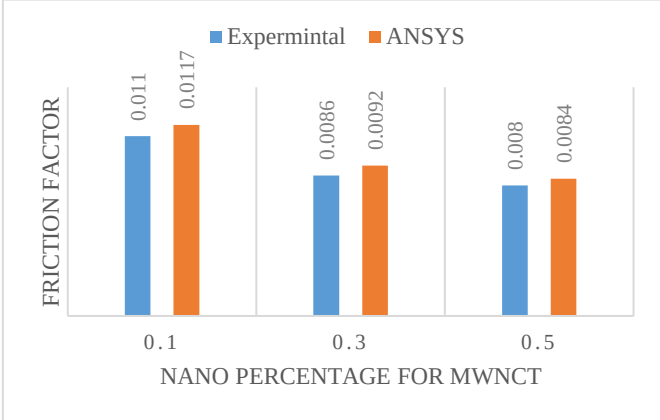

Figure 15. The friction factor of the three nanoparticles concentration

4. CONCLUSIONS

This study was performed using ANSYS FLUENT program for simulating cone helical coiled tube heat transfer properties and pressure drops, which were filled with 0.1%, 0.3%, and 0.5% MWCNT/water particle volume concentrations. The current research is devoted to ANSYS simulation that allows to conduct detailed investigation of pressure drop velocity

correlation. Flow rate conditions also had significant impact on pressure decrease. Pressure drop also increases with flow rate rises, due to higher dynamic pressure loss and turbulence flow enhancement inside curved pipe.

Moreover, nanofluids kept higher pressure downfall as they went through the heat exchanger with an increase rate of up to 3% as compared to water. High viscosity was the cause of high flow resistance which was due to the rise in viscosity caused by increased nanoparticle concentration in nanofluid. Nanofluids efficiency was measured by performance factor that was calculated using Nusselt number and pressure drop. The following points could be concluded from this work:

(1). ANSYS velocity calculation results demonstrated negligible differences in nanofluid velocity (0.1%, 0.3%, and 0.5%) across the three concentrations along the coil cross-sections. The observed differences in velocity values among the three tested sites were attributed to the alteration in coil curvature, which directly affects the velocity of the nanofluid. A reduction in the curvature of the helical coil leads to a rise in velocity at both the center and outlet sections. Conversely, heat exchanger between hot water outside and cold nanofluid inside coil results in elevation of temperature of nanofluid.

(2). Nanofluid density (multi-walled carbon nanotubes) in 0.1%, 0.3%, and 0.5% concentrations, exhibits straight proportionality to Dean number. Rises in particle volume concentration led to 26%, 49%, and 65% Nusselt number increases compared to water.

(3). In 0.1%, 0.3%, and 0.5% nanofluid concentrations, heat transfer coefficient enhancement was calculated to be 17%, 34%, and 47% higher than water, respectively. Evidence indicates that heat transfer coefficient reaches its maximum value at 0.5% nanofluid concentration. Increased amounts of multi-walled carbon nanotubes (MWCNT) led to enhanced thermal conductivity of nanofluids.

(4). Simulation results indicate that variation in particle volume concentration and Dean number leads to increase in pressure loss. Results suggest that pressure reductions achieved with 0.1%, 0.3%, and 0.5% nanofluid concentrations exceeded those of water by 18%, 33%, and 45% respectively. Dean's number or flow rate shows positive correlation with increasing pressure loss. Pressure drops exhibited proportional increase with rise in flow rate.

(5). Direct association seen between performance metric and concentration. These phenomena can be ascribed to concomitant rise in both pressure drops and Nusselt number, combined with improvement in heat transfer efficiency that is higher than rise in pressure drops. Performance factor measures contribution of increase in pressure drop of nanofluid to improved heat transfer efficiency.

REFERENCES

[1] Karamallah, A.A., Habeeb, L.J., Rahmah, N.M. (2016). Investigation of flow and heat transfer in a double pipe heat exchanger with nano fluid. Advances in Natural and Applied Sciences, 10(12): 8-16.

[2] Mahdi, A.S., Kalash, A.R., Suffer, K.H., Habeeb, L.J. (2020). Experimental and numerical investigation of heat transfer enhancement by using different geometry coiled tubes. Journal of Mechanical Engineering Research and Developments, 43(4): 92-104.

[3] Ali, A.J., Jaber, H.J., Habeeb, L.J., Tugolukov, E.N. (2020). Experimental investigation on the enhancement of heat transfer by using carbon nanotubes CNT taunit m series. IOP Conference Series: Materials Science and Engineering, 791(1): 012003. https://doi.org/10.1088/1757-899X/791/1/012003

[4] Shah, R.K., Joshi, S.D. (1987). Convective heat transfer in curved ducts. Handbook of Single-Phase Convective Heat Transfer, S. Kakac, R.K. Shah, W. Aung (Eds.), Wiley, New York, (Chapter 5) 5-3.

[5] Dean, W.R. (1928). The stream-line motion of fluid in a curved pipe. The London, Edinburgh, and Dublin Philosophical Magazine and Journal of Science, 5(30): 673-695. https://doi.org/10.1080/14786440408564513

[6] Figueiredo, A.R., Raimundo, A.M. (1996). Analysis of the performances of heat exchangers used in hot-water stores. Applied Thermal Engineering, 16(7): 605-611. https://doi.org/10.1016/1359-4311(95)00043-7

[7] Haraburda, S.S. (1995). Three-phase flow? Consider helical-coil heat exchangers. Chemical Engineering, 102(7): 149-151.

[8] Prasad, B.V.S.S.S., Das, D.H., Prabhakar, A.K. (1989). Pressure drop, heat transfer and performance of a helically coiled tubular exchanger. Heat Recovery Systems and CHP, 9(3): 249-256. https://doi.org/10.1016/0890-4332(89)90008-2

[9] Patil, R.K., Shende, B.W., Ghosh, P.K. (1982). Designing a helical-coil heat exchanger. Chemical Engineering, 89(25): 85-88.

[10] Rennie, T.J., Raghavan, V.G. (2006). Numerical studies of a double-pipe helical heat exchanger. Applied Thermal Engineering, 26(11-12): 1266-1273. https://doi.org/10.1016/j.applthermaleng.2005.10.030

[11] Jayakumar, J.S., Mahajani, S.M., Mandal, J.C., Iyer, K.N., Vijayan, P.K. (2010). CFD analysis of single-phase flows inside helically coiled tubes. Computers & Chemical Engineering, 34(4): 430-446. https://doi.org/10.1016/j.compchemeng.2009.11.008

[12] Cioncolini, A., Santini, L. (2006). On the laminar to turbulent flow transition in diabatic helically coiled pipe flow. Experimental Thermal and Fluid Science, 30(7): 653-661. https://doi.org/10.1016/j.expthermflusci.2006.01.004

[13] Choi, S.U., Eastman, J.A. (1995). Enhancing thermal conductivity of fluids with nanoparticles. (No. ANL/MSD/CP-84938; CONF-951135-29). Argonne National Lab.(ANL), Argonne, IL (United States). USA.

[14] Wai, O.J., Gunnasegaran, P., Hasini, H. (2022). A review on experimental and numerical investigations of jet impingement cooling performance with nanofluids. Micromachines, 13(12): 2059. https://doi.org/10.3390/mi13122059

[15] Nam, H.T., Cho, H.H., Lee, S., Lee, D. (2023). Temperature-dependent wicking dynamics and its effects on critical heat flux on micropillar structures in pool boiling heat transfer. International Communications in Heat and Mass Transfer, 146: 106887. https://doi.org/10.1016/j.icheatmasstransfer.2023.106887

[16] Bouselsal, M., Mebarek-Oudina, F., Biswas, N., Ismail, A.A.I. (2023). Heat transfer enhancement using Al_2O_3-MWCNT hybrid-nanofluid inside a tube/shell heat exchanger with different tube shapes. Micromachines, 14(5): 1072. https://doi.org/10.3390/mi14051072

[17] Akbari, M., Galanis, N., Behzadmehr, A. (2012). Comparative assessment of single and two-phase models

for numerical studies of nanofluid turbulent forced convection. International Journal of Heat and Fluid Flow, 37: 136-146. https://doi.org/10.1016/j.ijheatfluidflow.2012.05.005
[18] Sheikholeslami, M., Ebrahimpour, Z. (2022). Nanofluid performance in a solar LFR system involving turbulator applying numerical simulation. Advanced Powder Technology, 33(8): 103669. https://doi.org/10.1016/j.apt.2022.103669
[19] Kalteh, M., Abbassi, A., Saffar-Avval, M., Harting, J. (2011). Eulerian-Eulerian two-phase numerical simulation of nanofluid laminar forced convection in a microchannel. International Journal of Heat and Fluid Flow, 32(1): 107-116. https://doi.org/10.1016/j.ijheatfluidflow.2010.08.001
[20] Khosravi-Bizhaem, H., Abbassi, A. (2018). Effects of curvature ratio on forced convection and entropy generation of nanofluid in helical coil using two-phase approach. Advanced Powder Technology, 29(4): 890-903. https://doi.org/10.1016/j.apt.2018.01.005
[21] Kumar, N., Puranik, B.P. (2017). Numerical study of convective heat transfer with nanofluids in turbulent flow using a Lagrangian-Eulerian approach. Applied Thermal Engineering, 111: 1674-1681. https://doi.org/10.1016/j.applthermaleng.2016.08.038
[22] Kalb, C.E., Seader, J.D. (1972). Heat and mass transfer phenomena for viscous flow in curved circular tubes. International Journal of Heat and Mass Transfer, 15(4): 801-817. https://doi.org/10.1016/0017-9310(72)90122-6
[23] Zapryanov, Z., Christov, C., Toshev, E. (1980). Fully developed laminar flow and heat transfer in curved tubes. International Journal of Heat and Mass Transfer, 23(6): 873-880. https://doi.org/10.1016/0017-9310(80)90042-3
[24] Kozo, F., Yoshiyuki, A. (1988). Laminar heat transfer in a helically coiled tube. International Journal of Heat and Mass Transfer, 31(2): 387-396. https://doi.org/10.1016/0017-9310(88)90021-X
[25] Naphon, P., Suwagrai, J. (2007). Effect of curvature ratios on the heat transfer and flow developments in the horizontal spirally coiled tubes. International Journal of Heat and Mass Transfer, 50(3-4): 444-451. https://doi.org/10.1016/j.ijheatmasstransfer.2006.08.002
[26] Bae, S.W., Jeong, J.J., Chang, S.K., Cho, H.K. (2007). Two phase flow models and numerical methods of the commercial CFD codes. Korea Atomic Energy Research Institute: Daejeon, Republic of Korea.
[27] Wen, C.Y. (1966). Mechanics of fluidization. In Fluid Particle Technology, Chem. Eng. Progress. Symposium Series, 62: 100-111.
[28] Popiel, C.O., Wojtkowiak, J. (1998). Simple formulas for thermophysical properties of liquid water for heat transfer calculations (from 0°C to 150°C). Heat Transfer Engineering, 19(3): 87-101. https://doi.org/10.1080/01457639808939929
[29] Brinkman, H.C. (1952). The viscosity of concentrated suspensions and solutions. The Journal of Chemical Physics, 20(4): 571. https://doi.org/10.1063/1.1700493
[30] Gnielinski, V. (1976). New equations for heat and mass transfer in turbulent pipe and channel flow. International Chemical Engineering, 16(2): 359-367.
[31] Bianco, V., Manca, O., Nardini, S. (2011). Numerical investigation on nanofluids turbulent convection heat transfer inside a circular tube. International Journal of Thermal Sciences, 50(3): 341-349. https://doi.org/10.1016/j.ijthermalsci.2010.03.008
[32] El Bécaye Maïga, S., Tam Nguyen, C., Galanis, N., Roy, G., Maré, T., Coqueux, M. (2006). Heat transfer enhancement in turbulent tube flow using Al_2O_3 nanoparticle suspension. International Journal of Numerical Methods for Heat & Fluid Flow, 16(3): 275-292. https://doi.org/10.1108/09615530610649717
[33] Khanafer, K., Vafai, K., Lightstone, M. (2003). Buoyancy-Driven heat transfer enhancement in a two-dimensional enclosure utilizing nanofluids. International Journal of Heat and Mass Transfer, 46(19): 3639-3653. https://doi.org/10.1016/S0017-9310(03)00156-X
[34] Palanisamy, K., Kumar, P.M. (2019). Experimental investigation on convective heat transfer and pressure drop of cone helically coiled tube heat exchanger using carbon nanotubes/water nanofluids. Heliyon, 5(5): e01705. https://doi.org/10.1016/j.heliyon.2019.e01705